Received 8 May 2022; revised 13 June 2022; accepted 18 June 2022. Date of publication 22 June 2022; date of current version 6 July 2022.

Digital Object Identifier 10.1109/OJAP.2022.3185462

A Pattern-Reversal Wideband Antenna Integrating Metal Rings, Diodes-Loaded Stubs and Defective Ground

YU LIU[1,2], LI-AN BIAN[1,2], KAI-DA XU[3,4] (Senior Member, IEEE), KAICHENG HUANG[1,2], YAOKUN WANG[1,2], YANXIU LI[1,2], AND SHU XIE[1,2]

[1]School of Physics and Electronic Science, Changsha University of Science and Technology, Changsha 410114, China

[2]Hunan Province Higher Education Key Laboratory of Modeling and Monitoring on the Near-Earth Electromagnetic Environments, Changsha University of Science and Technology, Changsha 410114, China

[3]School of Information and Communications Engineering, Xi'an Jiaotong University, Xi'an 710049, China

[4]State Key Laboratory of Precision Spectroscopy, East China Normal University, Shanghai 200241, China

CORRESPONDING AUTHORS: L.-A. BIAN and K.-D. XU (e-mail: dk061bianlian@126.com; kaidaxu@ieee.org)

This work was supported in part by the Scientific Research Fund of Hunan Provincial Education Department under Grant 21B0278; in part by the Practical Innovation Plan of Changsha University of Science and Technology under Grant SJCX202191; in part by the State Key Laboratory of Advanced Optical Communication Systems Networks under Grant 2022GZKF020; and in part by the State Key Laboratory of Precision Spectroscopy Open Research Program.

ABSTRACT The pattern reconfigurable antenna provides a new implementation scheme for expanding application in modern wireless communications. In this paper, a pattern-reversal wideband microstrip antenna is proposed. This antenna is composed of a radiation patch with attached rectangular metal rings connected by a microstrip line on the upper layer and a four-defects ground plane connecting two PIN-diodes-loaded L-shaped stubs on the bottom layer. In view of the Yagi-antenna feature of metal rings and L-shaped stubs, the ON-OFF of diodes controls directly the radiation direction of antenna. Under the joint action of multiple resonances of rings, slots and stubs, the bandwidth of antenna is surged so as to develop evident wideband radiation. Finally, the measured impedance bandwidth of -10 dB is about 20.1% from 4.54 to 5.55 GHz. The average gain of the antenna with the size of $0.75\lambda_0 \times 0.75\lambda_0$ reaches 4.92 dBi. With the diodes dependence, the pattern can really deflect in opposite direction. The designed antenna has much advantages, such as low cost, wider band, compact and simple structure along with explicit application scenarios.

INDEX TERMS Microstrip antenna, wideband, pattern reversal, PIN diodes, defective ground.

I. INTRODUCTION

WITH the rapid development of contemporary wireless communication systems, higher requirements are put forward for the performance of indispensable antennas, which are mainly reflected in the wider working frequency band, smaller size, easier installation and integration along with higher radiation efficiency. In order to improve communication security and efficiency as well as reduce the antagonistic effect of co-channel interference and channel blockage, pattern reconfigurable antennas are usually required in some application scenarios, such as satellite communications, medical devices and other fields.

In the recently reported works, the methods to realize the pattern reconfiguration are roughly divided into the following three types. The first one is to change the structure of the antenna. References [1] and [2] mechanically altered the geometry of the antenna to realize pattern tuning. This way will introduce large mechanical errors and is not suitable for the field of miniaturized civil mobile communications. The second one is to use special materials to obtain the reconfigurable pattern. To achieve beam control, [3]–[6] used the shape memory alloy, the distilled water parasitic unit and the graphene film. In [7], the liquid metal antenna adopted room temperature liquid eutectic gallium-indium

(EGaIn) alloy to realize bidirectional directional radiation. Reference [8] introduced an arched water column around the seawater monopole antenna as a parasitic passive oscillator to realize dual beam radiation, wide-angle radiation and directional high gain radiation. In [9], the antenna was made of highly flexible PDMS conductive fabric composite. Overall, the use of special materials is generally complicated and costly, and thus it is hard to be widely employed in actual production. The last one is to switch the feed network of the antenna. References [10]–[19] all changed the current distributions on the patch by controlling the ON-OFF state of the integrated PIN the integrated PIN diodes on the antenna to realize the manipulation of pattern. Reference [20] controlled the phase difference between the fields at the two radiation slots to reorganize the beams. Reference [21] achieved the beam reconfiguration by selecting the appropriate excitation port combination for the slot patch with double-sided frequency selective surface. Reference [22] proposed a microstrip switchable double balun with symmetrical three-coupling-line structure as the feed network to design the radiation mode reconfigurable end-fire antenna. Reference [23] used a microcontroller to switch the array of cubes excited by the feed network. By selecting a specific mode on the mobile application, the radiation mode of the array is reconfigured. Comparatively, the third method is more realistic, but these mentioned antennas have either a narrow working bandwidth in [10], [11], [18]–[20], or low gain in [14]–[17], or complex and bulky structures which are not easy to integrate in [12], [13], [21]–[23].

In this paper, a reconfigurable wideband microstrip antenna is proposed. Two diodes are embedded into the L-shaped stubs on the ground contribute directly to the reconfigurability. Then, the wideband performance is realized by jointing the metal rings next the patch on the upper plane and four slots on the lower plane of antenna. Based on the Yagi-antenna property of metal-rings and L-shaped branches, the pattern is reversible. Simulated and measured results are almost coincident, showing that this antenna has indeed a wider impedance bandwidth, higher gain and better beam deflection ability.

II. ANTENNA DESIGN AND ANALYSIS

A. STRUCTURE OF ANTENNA

Fig. 1 shows the geometry of the pattern-reconfiguration antenna. The dielectric substrate is Rogers RO4350B with the relative permittivity of 3.48 and the loss tangent of 0.0037. The size of the entire antenna is $45(0.75\lambda_0)$mm $\times$ $45(0.75\lambda_0)$mm $\times$ $0.762(0.0127\lambda_0)$mm, where λ_0 is the corresponding wavelength of 5GHz in free space. The upper layer of the dielectric substrate is the radiation surface of the antenna, where mainly a rectangular patch is connected to two rectangular metal rings through a microstrip line. The antenna is fed by a microstrip transmission line with a characteristic impedance of 50 Ω. On the lower layer of substrate, the ground plane consists of two parts. The first part is a rectangle sheet etched with four defective ground structures (DGS), including a pair of symmetrical C-slots in the X-axis direction and two triangular slots in the Y-axis direction. The second part is a symmetrically distributed L-shaped stubs with the embedded PIN diodes. The parameter values after optimization are shown in Table 1.

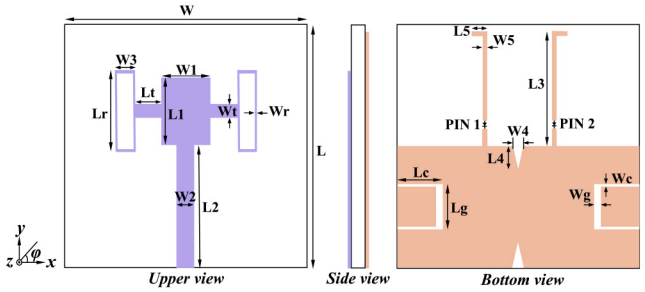

FIGURE 1. Geometry of the proposed antenna.

TABLE 1. Optimized parameters of this antenna (Units: mm).

Parameter	Value	Parameter	Value	Parameter	Value
W	45.0	W1	9.0	W2	3.0
W3	3.6	W4	2.0	W5	1.0
Wr	0.3	Wg	1.2	WC	0.5
Wt	2.5	L	45	L1	12.5
L2	22.2	L3	21.6	L4	5.0
L5	7.8	Lr	15.0	Lc	8.3
Lg	8.3	Lt	5.0		

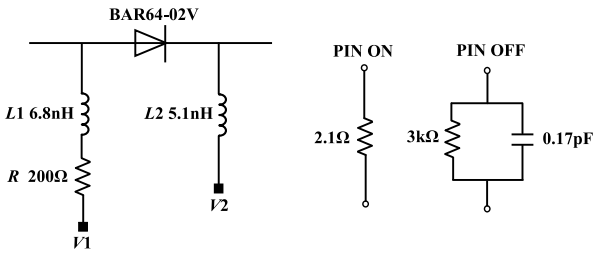

FIGURE 2. Biasing circuit for PIN diodes.

The antenna can realize pattern reconfiguration by changing the working states of the PIN diodes. A PIN diode is often equivalent to such a circuit composed of the capacitor and resistor in the RF field for the convenience of study. The diode bias is controlled by the DC bias circuit as given in the Fig. 2. In order to isolate RF signals from DC signals as much as possible, additional inductors are added to the circuit. A biasing voltage of 3V or 0V is applied to the bias circuit for the switch ON or switch OFF condition. Two operating states of the antenna are given in Table 2. In view of the high degree of symmetry of antenna structure, the working frequency band of the antenna is basically the same in the two states. Hence, State 1 is only considered here as an example to analyze this antenna performance.

The equivalent circuit of designed antenna is displayed in Fig. 3. The rectangular radiation patch is equivalent to a *RLC* lossy parallel resonant circuit composed of R_a, C_a

TABLE 2. Operating states of the antenna.

Operating States	PIN 1	PIN 2
State 1	ON	OFF
State 2	OFF	ON

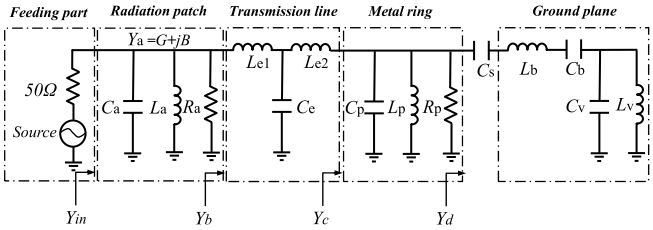

FIGURE 3. Equivalent circuits of designed antenna.

and L_a. Then, the expression of input admittance Y_a can be obtained as

$$Y_a = \frac{1}{R_a} + j\omega C_a + \frac{1}{j\omega L_a} \tag{1}$$

in which R_a, C_a and L_a can be known from [24]. The microstrip transmission line is equivalent to a lossless resonant circuit composed of two series inductors of L_{e1} and L_{e2} along with a parallel capacitor C_e [25]. Furthermore, the rectangular metal ring is equivalent to a *RLC* lossy parallel resonant circuit composed of R_p, L_p and C_p [26]. The ground plate is composed of L-shaped branches and defective ground structure, so it is equivalent to a parallel and series *LC* resonant circuit with L_b, C_b, C_v and L_v [27]. Besides, C_s is the coupling capacitance between the radiation patch and the ground plate. By utilizing these local admittance as provided by Eqs. (1)-(4), the input admittance Y_{in} of the whole equivalent circuit can be gained based on Eq. (5). Ultimately, the electrical parameters are optimized as $C_a = 1.1$pF, $L_a = 1.1$nH, $R_a = 129\Omega$, $L_{e1} = 0.32$nH, $C_e = 0.68$pF, $L_{e2} = 0.39$nH, $C_p = 0.8$pF, $L_p = 0.5$nH, $R_p = 78\Omega$, $C_s = 1.2$pF, $C_b = 1.1$pF, $L_b = 0.9$nH, $C_v = 0.25$pF and $L_v = 13$nH. Evidently, the resonance of equivalent circuit can be controlled by adjusting the size of antenna and then the bandwidth could be broadened depending on the resonance coupling.

$$Y_b = \left[j\omega L_{e1} + \left(\frac{1}{j\omega L_{e2}} + j\omega C_e \right)^{-1} \right]^{-1} \tag{2}$$

$$Y_c = \frac{1}{R_p} + j\omega C_p + \frac{1}{j\omega L_p} \tag{3}$$

$$Y_d = \left[j\omega L_b + \frac{1}{j\omega C_s} + \frac{1}{j\omega C_b} + \left(j\omega C_v + \frac{1}{j\omega L_v} \right)^{-1} \right]^{-1} \tag{4}$$

$$Y_{in} = Y_a + Y_b + Y_c + Y_d. \tag{5}$$

B. EVOLUTION AND COMPARISON OF ANTENNAS

Fig. 4 and 5 present the evolution structures of upper plane and ground plane of antennas. A typical microstrip antenna utilizes often rectangular patch in Fig. 4(a), whose frequency

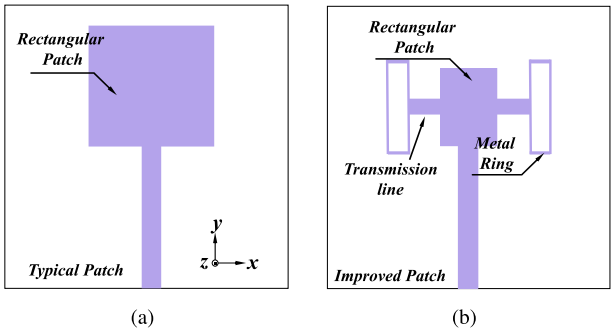

FIGURE 4. Upper plane with (a) typical patch, (b) metal-rings-loaded patch.

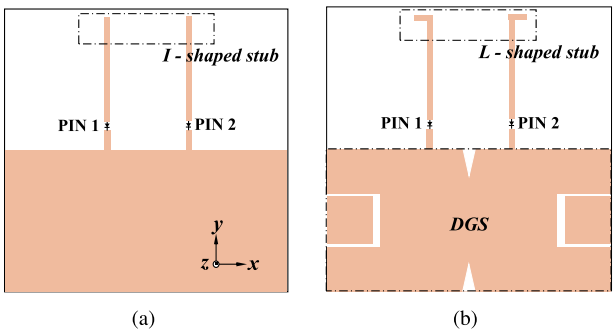

FIGURE 5. Ground plane with (a) I-shaped stubs, (b) L-shaped stubs and DGS.

band is narrow with the bandwidth from 3% to 5% due to the high Q property. In order to expand the bandwidth and meanwhile enhance the directivity of antenna, a pair of rectangular metal rings as the deflectors with reactance feature are added on both sides of the traditional patch in Fig. 4(b), where the metal rings and the patch are connected by the transmission line. The ground plane of the initial design is revealed in Fig. 5(a), where two diodes are embedded into the I-type branch to realize the reconfiguration of pattern. To obtain wider bandwidth, a pair of C-shaped grooves and a pair of triangular grooves are introduced to form the DGS, and a parasitic branch is added to the I-shaped branch to develop the L-shaped one in Fig. 5(b). Fig. 6 shows these four antennas through the combination of those in Fig. 4 and Fig. 5.

Fig. 7 shows the surface current distributions of Ant 1 and Ant 2 at 5.0GHz in State 1. Clearly, the surface current of Ant 1 mainly distributes on the I-type branch of the bottom ground, and the current of a single patch on the upper layer is relatively weak. The surface current of Ant 2 is mainly concentrated on the rectangular metal ring on the left, while the metal ring on the right has only a little current. The right ring is equivalent to a parasitic unit as the reflector to reflect the radiation energy to the left one so as to enhance the directivity of the antenna. Fig. 8 displays the 2-D radiation of Ant 1 and Ant 2 on the *xoy* plane at varying frequencies. Obviously, the radiation pattern of Ant 2 is more stable against the change of frequency, which

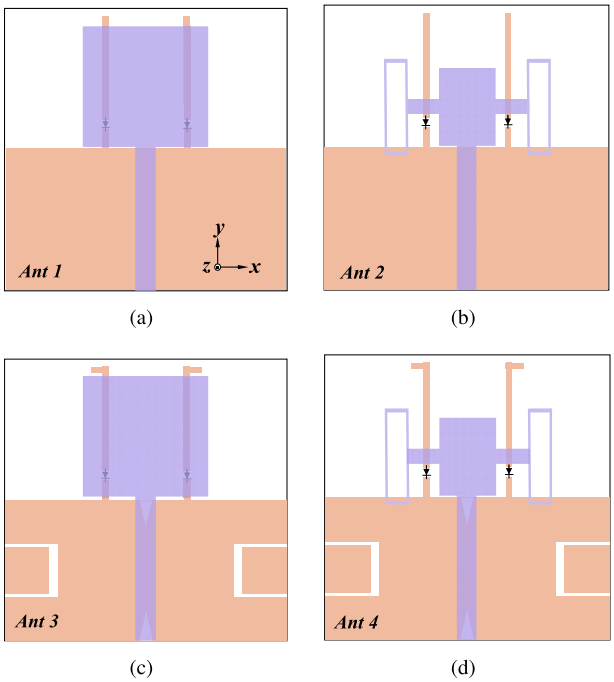

FIGURE 6. Geometry of the antenna with (a) typical patch and the ground plane with I-shaped stubs (Ant 1), (b) metal-rings-loaded patch and the ground plane with I-shaped stubs (Ant 2), (c) typical patch and the ground plane with L-shaped stubs and DGS (Ant 3), (d) metal-rings-loaded patch and the ground plane with L-shaped stubs and DGS (Ant 4).

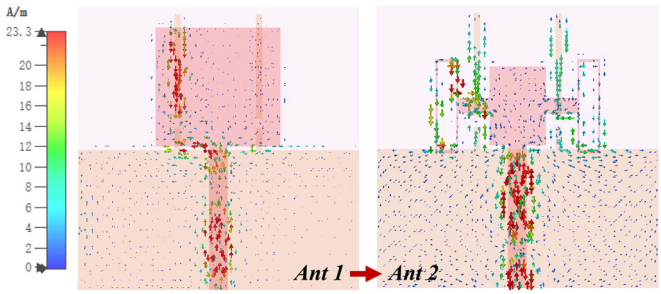

FIGURE 7. Surface current distributions of Ant 1 and Ant 2 at 5.0 GHz.

indicates that the antenna directivity can be improved really by adding two metal rings.

In order to further study the effect of the right metal ring as the reflector on the antenna radiation, the structure of the Ant 2 without the right ring and corresponding pattern are given in Fig. 9. As seen, when the antenna does not have a reflective metal ring, the radiation pattern also deflects to the left with the diode in ON state. However, the effect is not obvious and the back lobe is large. Moreover, the gain is only 1.74dBi at 5.0GHz. Instead, when the antenna has the reflective metal ring on the right, the pattern deflects to the left metal ring obviously, and the gain increases to 5.76dBi at 5.0GHz as presented in Fig. 8(b).

Fig. 10 shows the reflection coefficients for Ant 3 and Ant 4 with different ground structures. The panel (a) displays the results with and without DGS, where the inset presents the ground without DGS. As seen, the position of deepest dip is

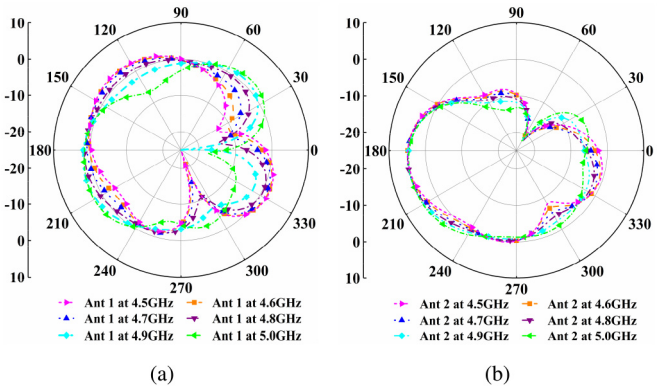

FIGURE 8. Simulated 2-D radiation of (a) Ant 1 and (b) Ant 2 in the *xoy* plane.

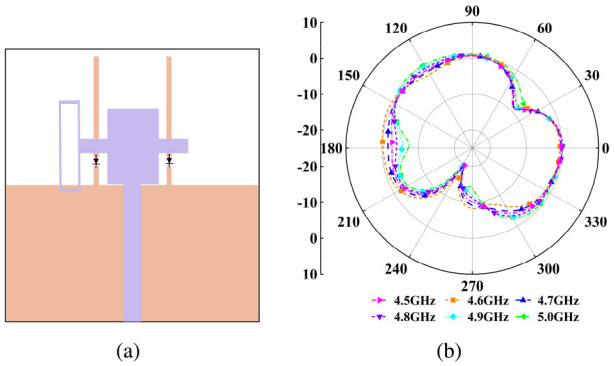

FIGURE 9. Simulated 2-D radiation of Ant 2 without right reflective metal ring in the *xoy* plane. (a) Ant 2 without right metal ring. (b) Corresponding 2-D radiation pattern.

basically unchanged in both cases, but the impedance bandwidth with DGS is much broader than that without the one. This is because that there is a dense current distribution near the DGS, and a new resonance dip can be generated near the original one by adjusting the size of DGS. Then, the bandwidth is expanded based on the resonance coupling. The panel (b) displays the results with different-shape stubs, where the ground with I-shaped stubs is given in the inset. For the convenience of design and processing, the antenna usually uses I-shaped branch [28]. However, the L-shaped one is used here in order to obtain a wider impedance bandwidth. The reflection coefficient and impedance bandwidth of the antenna with L-shaped stubs are much better than those with I-shaped ones. The main reason is that the L-shaped stub has two parasitic units compared with the I-shaped stub. Through the method similar to staggered tuning, the new resonant dip is located near the original one. The coupling of all resonant modes contributes to better impendence matching, and thus improves the bandwidth of the antenna.

The comparison of different evolutionary models is shown in Fig. 11. In the panel (a), the bandwidth of Ant 2 with metal-rings-loaded patch increases slightly from 246MHz to 384MHz relative to Ant 1 with typical rectangular patch. Meanwhile, Ant 3 with L-shaped branch and DGS shows also better bandwidth characteristic, which has more than twice the bandwidth compared with Ant 1. In a word, both

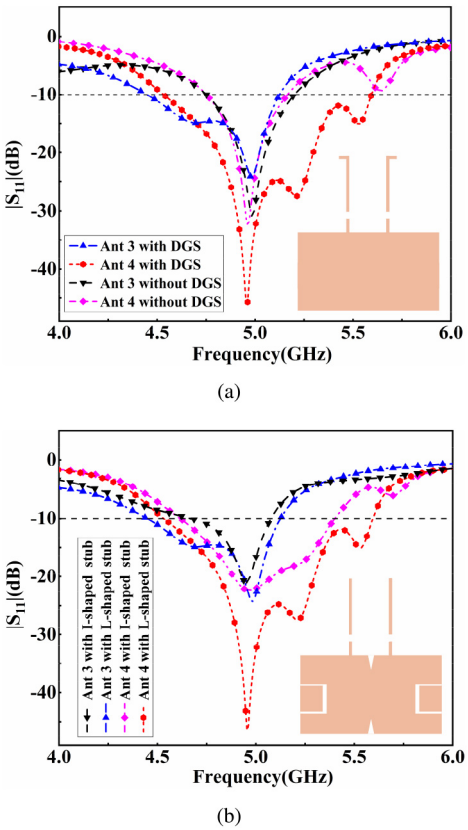

FIGURE 10. Reflection coefficients for varying ground structures. (a) With or without the DGS. (b) With I-shaped or L-shaped stubs.

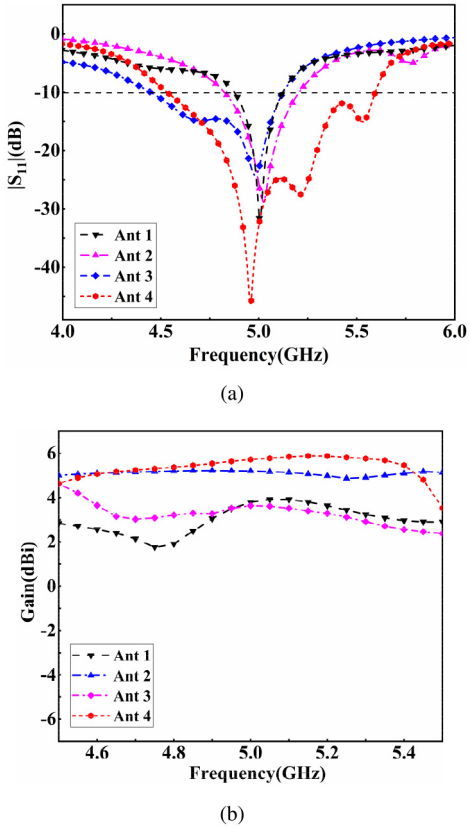

FIGURE 11. Simulated results of Ant 1, 2, 3, 4. (a) S11. (b) Gain.

Ant 2 with the improved patch and Ant 3 with the improved ground plane show better impedance characteristics than Ant 1. As a result, Ant 4 with both improved patch and ground has a wider bandwidth. In the panel (b), there is not much difference between the Ant 1 and Ant 3 at higher frequencies and Ant 2 and Ant 4 at lower frequencies with the same patches and different grounds. However, the gain of the antenna with the same ground plane and different radiation patches is quite different. The main reason is that relative to the traditional simple patch, the two extra metal rings act separately as director unit and reflector unit, revealing Yagi-antenna feature, which makes the electromagnetic energies more concentrated so as to greatly enhance the directivity of the antenna. In short, Ant 4 has the best performance with the deepest dip of -46.373 dB, the widest bandwidth of 1030MHz and the maximum gain of 5.89dBi.

C. PARAMETRIC ANALYSIS

The variation of antenna parameters will affect directly antenna performance, especially the geometries of the mental rings, transmission line, slots and stubs restricting the wide-band characteristic. This section will still take State 1 as an example to give important analyses to better comprehend the parameter dependence of antenna.

Fig. 12 shows the effect of the width Wt of the transmission line as a bridge connecting the metal ring and the center patch and the length Lr of the metal ring on the upper plane of antenna. In the panel (a), the imperfect matching impedance leads to a small stopband when Wt is 2.0mm. With the increase of Wt, the impedance matching is improved so that the resonance dip deepens and meanwhile shifts to the left, which brings about that the stopband disappears and a wider bandwidth is obtained when Wt is 2.5mm. As the Wt increases to 3.0mm, the impedance matching deteriorates again, triggering that the resonant dip moves up and the bandwidth becomes narrow. In the panel (b), Lr affects strongly the resonance of antenna, since Lr determines the reactance characteristics of the metal rings. The ring is equivalent to the *RLC* circuit, so the second resonance dip of appears at about 5.75GHz when Lr is 13 mm. With the increase of Lr, the resonance frequency decreases and the third mode is excited when Lr becomes 15mm. Through the coupling of three modes, more frequencies satisfy the condition of $|S_{11}| < -10$dB. As the Lr increases further to 17mm, a stopband emerges and then the bandwidth worsens accordingly. Therefore, attaching appropriately metal rings next the patch can quite expand bandwidth.

Fig. 13 depicts the influence of the depth Lc of C-slot and the width W5 of L-shaped stub on the lower plane of antenna. In the panel (a), when the Lc is 8.0mm, there are three resonant dips. However, the distance between each other is great, so the antenna bandwidth is not improved. As the Lc increases to 8.3mm, three resonant dips become

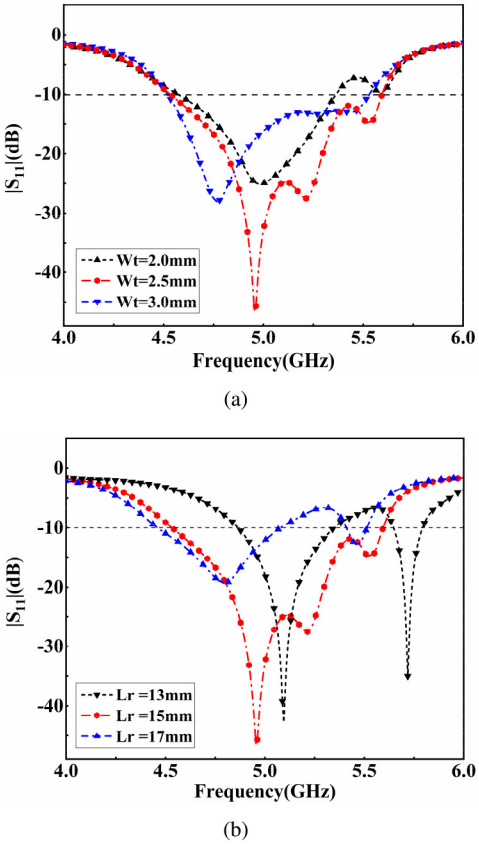

FIGURE 12. Reflection coefficients against the change of (a) Wt, (b) Lr.

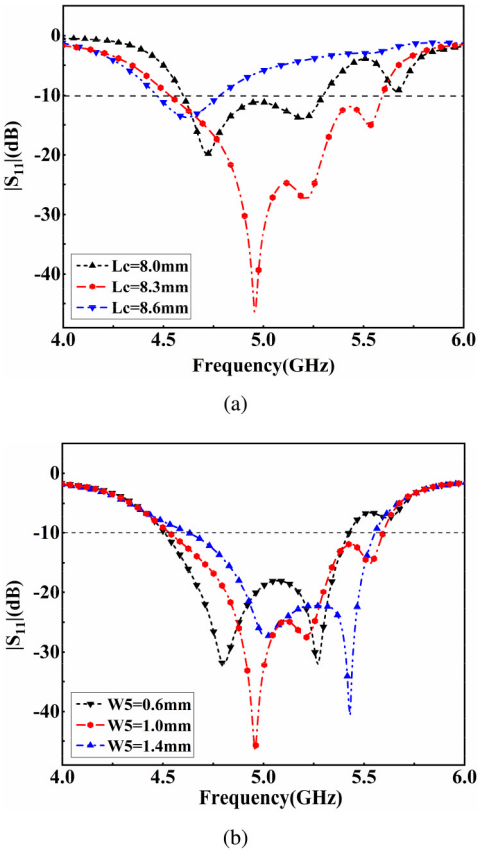

FIGURE 13. Reflection coefficients against the change of (a) Lc, (b) W5.

closer so that the resonant coupling is strong enough to pull down the S_{11} in a wider range. With the increase of Lc to 8.6 mm, the second resonance moves far away from the fundamental resonance, which causes impedance mismatching at target frequencies.In the panel (b), the width of W5 has a significant impact on the impedance bandwidth and resonance frequency. This is because the L-shaped stub extremely affects the coupling between the radiation patch and the ground plane. When the W5 is 0.6mm, the antenna appears two dips. As the W5 increases to 1 mm, a third dip is achieved and then a large band arises. With the increase of W5 to 1.4mm, the dips number turns into two once more resulting in a narrower bandwidth. Therefore, the effective introduction of slot and stub is very important to wideband radiation.

D. OPERATING PRINCIPLE OF PATTERN REVERSAL

This section will elaborate on the realization mechanism of pattern reversal. The current distribution in each state is shown in Fig. 14. From the panel (a), the current on the upper plane is mainly distributed on the left rectangular metal ring, indicating that the antenna is affected by the left part in State 1. The current on the lower plane distributes mainly in the L-shaped stub with conductive diode. Also, this current is concentrated around the left C-slot near PIN 1 and two triangular slots. Instead, there is little current around the right C-slot away from PIN 1. From the panel (b), the opposite case happens in State 2. On the whole, there is also weak current distribution on the stub with the non-conducting diode due to the coupling effect. Currently, the disconnected stub is equivalent to a parasitic element acting as a reflector, reflecting the radiated energy to the direction of another stub with ON-state diode, whose mechanism is analogue to Yagi antenna. Hence, the function of pattern reversal can be realized by manipulating the ON-OFF state of the PIN diode.

Fig. 15 describes the E-field distributions with different phases on the substrate in State 1. At the 45°, the E-fields are distributed mainly on the rectangular patch, the left metal ring and C-slot and a few fields are on the right L-shaped stub. At the 135°, the E-fields are most localized at the patch, the left metal ring and L-shaped stub, and slight fields are on the right metal ring. Obviously, the E-fields on the left-right symmetrical patches, metal rings, C-slots and L-shaped stubs are different, which is not symmetrical about the *X*-axis, resulting in the deviation of the main beam from the *Z*-axis. Instead, the E-fields in State 2 are distributed nearly in opposite positions, which results in opposite direction deflection of pattern.

III. MEASURED RESULTS AND DISCUSSIONS

In order to verify the effectiveness of the design method and explore the consistency between the simulation and

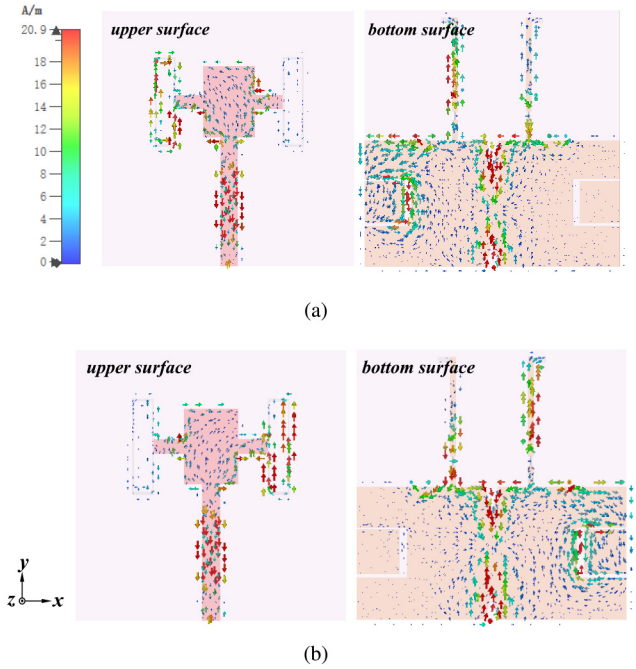

FIGURE 14. Current distribution in each operating state. (a) State 1. (b) State 2.

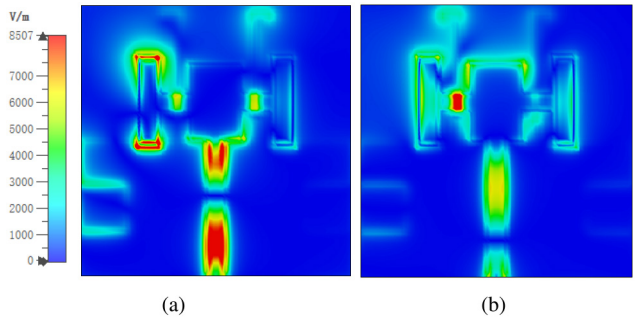

FIGURE 15. E-field distributions on the substrate in State 1 with phases of (a) 45° and (b) 135°.

measurement results, the antenna is manufactured. The corresponding electronic components are welded on the antenna and the diodes' bias circuit is built according to the foregoing analysis. Fig. 16 gives the manufactured antenna and test scenario, where the bias voltage is provided by the bias circuit for the PIN diodes through two 1.5V dry batteries, and the vector network analyzer of Agilent company and the microwave darkroom are used for antenna measurement.

Fig. 17 displays the comparison results between the simulation and measurement in two states. In the panel (a), the simulated and measured impedance bandwidth are about 21.4% (4.53-5.6GHz) and 20.1% (4.54-5.55GHz), which are consistent basically. Merely, the measured results are slightly inferior to the simulation ones because of the inevitable machining tolerance and the insertion loss of the DC bias circuit introduced by the external antenna. In the panel (b), the gain is flat in general with the dynamic range of 1dB for both results, and the overall gain effect is high. Evidently, the antenna gain suffers from little influence of the stopband.

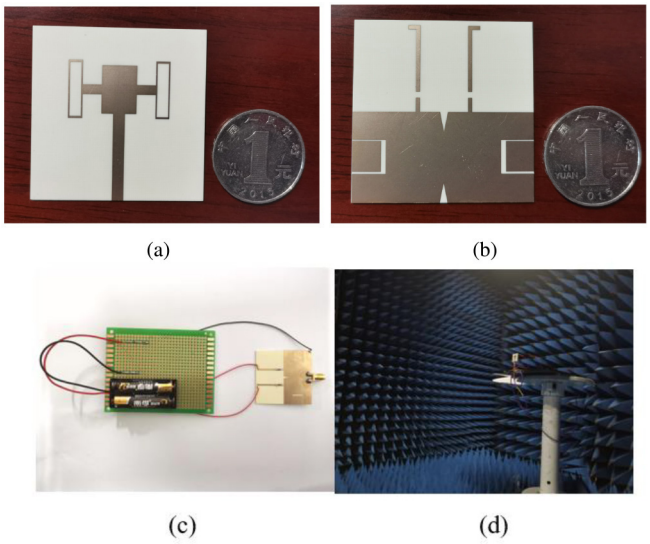

FIGURE 16. Manufactured antenna and test scenario. (a) Upper side of antenna. (b) Bottom side of antenna. (c) Antenna with DC circuit. (d) Test scenario.

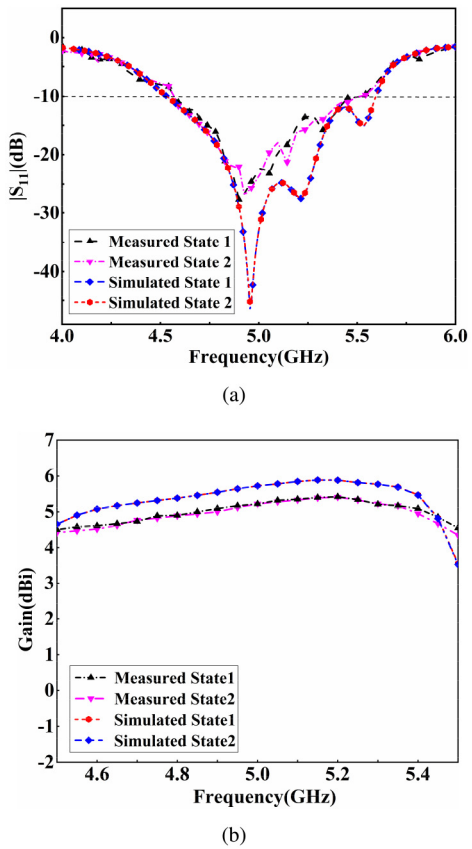

FIGURE 17. Simulated and measured results in two states. (a) S11. (b) Gain.

The simulated average gain is 5.34dBi, while the measured average gain becomes 4.92dBi. It reduces about 0.42dBi caused by the insertion loss of the bias circuit and the SMA connector, which is within a reasonable range.

The simulated and measured co-polarization and cross-polarization of the radiation pattern in azimuth plane (*xoy*

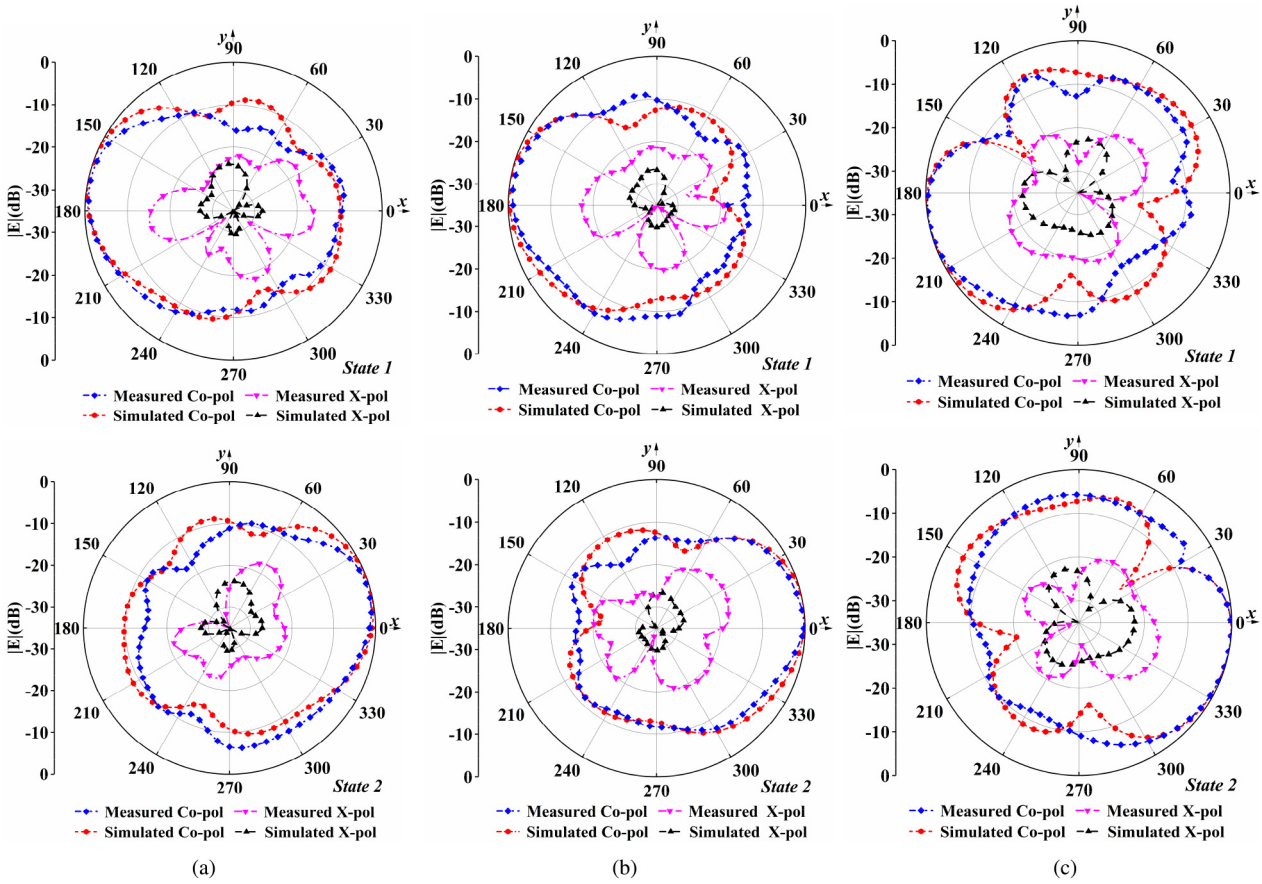

FIGURE 18. Simulated and measured radiation patterns in the *xoy* plane. (a) 4.55 GHz, (b) 5.0 GHz, (c) 5.55 GHz.

TABLE 3. Comparison between this work and previously published antennas.

Ref.	Size($\lambda_0{}^2$)	No. of Modes	No. of Diodes	Bandwidth	Peak Gain
[10]	0.72 × 0.54	3	16	430MHz15.2%	6.4dBi
[11]	1.17 × 1.17	4	8	190MHz5.6%	6.7dBi
[12]	0.82 × 0.78	9	8	60MHz2.5%	6.3dBi
[14]	0.624 × 0.624	4	4	1000MHz26.3%	3.3dBi
[15]	0.48 × 0.62	4	4	760MHz34%	4.0dBi
[16]	0.37 × 0.37	2	2	670MHz30.2%	4.54dBi
[17]	0.22 × 0.27	3	2	860MHz41.3%	2.2dBi
[21]	0.82 × 0.82	8	4	210MHz11.6%	8.4dBi
[22]	0.51 × 0.98	3	4	100MHz4.92%	5.8dBi
This work	0.75 × 0.75	2	2	1010MHz20.1%	5.42dBi

plane) are revealed in Fig. 18. It can be observed that the radiation main beam on azimuth plane is determined by the working state of the antenna. The pattern is relatively stable which can be reconstructed in two opposite directions. With the suitable arrangements of the bias voltage, the maximum beam direction deflection was $\varphi = 162°$ and $\varphi = 18°$ at 4.55 GHz, $\varphi = 172°$ and $\varphi = 8°$ at 5.0 GHz, $\varphi = 188°$ and $\varphi = 352°$ at 5.55 GHz respectively. Obviously, in the whole impedance bandwidth, this antenna can realize the reversal of pattern. Besides, the radiation of antenna maintains a good directionality against varying frequency, which is suitable for such communication systems demanding well anti-interference ability.

The performance comparison between this work and other published beam-reconfiguration antennas is shown in Table 3. The antennas in [10]–[12], [21] and [22] have higher gain, but they own narrower bandwidth. Meanwhile, the size of antennas in [11], [12] and [21] is larger. The antennas in [14]–[17] have a wider bandwidth and smaller size, but their gains are not high. Therefore, the antennas mentioned above either have too narrow working bandwidth, too low gain, or too large size to be utilized conveniently, which cannot well meet the requirements of wide band, high gain and small size in the contemporary wireless communication system. Further, although there are more number of reconfigurable modes in [10]–[12], [14], [15], [21] and [22], more diodes are utilized, which makes the antenna structure more complex. The comparison results show that the proposed antenna has a compact structure, wide bandwidth and good gain characteristics as a whole, which can improve effectively the quality and capacity of the communication system.

IV. CONCLUSION

A wideband microstrip antenna with the reversible pattern is proposed in this paper. This antenna is compact with the size of $0.75\lambda_0 \times 0.75\lambda_0$. Specifically, two PIN diodes as

controllable devices are loaded on the L-shaped stubs. And rectangular metal rings, C-shaped slots and triangular slots are integrated into the upper and lower plane of antenna. Depending on the states of diodes and the Yagi-antenna property of structure, the pattern can deflect inversely. Relaying on the multi-resonance at the patch and ground, the radiation band is enhanced greatly. Measured results show that the impedance bandwidth reaches 20.1% from 4.54GHz to 5.55GHz and the average gain is 4.92dBi in the band range. Meanwhile, the deflection angle of maximum beam reaches 164° at the center frequency of 5GHz. Based on the reversible pattern, the wideband antenna could be used in anti-reference communications, aircraft multi-directional tracking and multi-target radar imaging.

REFERENCES

[1] P. K. Li, C. J. You, H. F. Yu, and Y. J. Cheng, "Mechanically pattern reconfigurable dual-band antenna with omnidirectional/directional pattern for 2.4/5GHz WLAN application," *Microw. Opt. Technol. Lett.*, vol. 59, no. 10, pp. 2526–2531, Mar. 2017.

[2] I. T. Nassar, H. Tsang, D. Bardroff, C. P. Lusk, and T. M. Weller, "Mechanically reconfigurable, dual-band slot dipole antennas," *IEEE Trans. Antennas Propag.*, vol. 63, no. 7, pp. 3267–3271, Jul. 2015.

[3] L. Sumana and S. E. Florence, "Pattern reconfigurable microstrip patch antenna based on shape memory alloys for automobile applications," *J. Electron. Mater. Lett.*, vol. 49, no. 11, pp. 6598–6610, Sep. 2020.

[4] Y.-H. Qian and Q.-X. Chu, "A pattern-reconfigurable water-loaded MIMO antenna," *Microw. Opt. Technol. Lett.*, vol. 59, no. 7, pp. 1608–1613, 2017.

[5] K. Moradi, A. Pourziad, and S. Nikmehr, "An efficient graphene-based reconfigurable terahertz ring antenna design," *AEU-Int. J. Electron. Commun.*, vol. 149, May 2022, Art. no. 154177.

[6] B. Zhang and K.-D. Xu, "Switchable and tunable bifunctional THz metamaterial absorber," *J. Opt. Soc. America B*, vol. 39, no. 3, pp. A52–A60, 2022.

[7] J. Hao, J. Ren, X. Du, J. H. Mikkelsen, M. Shen, and Y. Z. Yin, "Pattern-reconfigurable Yagi-Uda antenna based on liquid metal," *IEEE Antennas Wireless Propag. Lett.*, vol. 20, no. 4, pp. 587–591, Apr. 2021.

[8] Y. Yang *et al.*, "A broadband reconfigurable antenna with parasitic water radiation array," *Int. J. RF Microw. Comput.-Aided Eng.*, vol. 31, no. 10, Jul. 2021, Art. no. e22824.

[9] B. Mohamadzade *et al.*, "A conformal, dynamic pattern-reconfigurable antenna using conductive textile-polymer composite," *IEEE Trans. Antennas Propag.*, vol. 69, no. 10, pp. 6175–6184, Oct. 2021.

[10] J. Ren, X. Yang, J. Yin, and Y. Yin, "A novel antenna with reconfigurable patterns using H-shaped structures," *IEEE Antennas Wireless Propag. Lett.*, vol. 14, pp. 915–918, 2015.

[11] W.-Q. Deng, X.-S. Yang, C.-S. Shen, J. Zhao, and B.-Z. Wang, "A dual-polarized pattern reconfigurable yagi patch antenna for microbase stations," *IEEE Trans. Antennas Propag.*, vol. 65, no. 10, pp. 5095–5102, Oct. 2017.

[12] Z.-L. Lu, X.-X. Yang, and G.-N. Tan, "A multidirectional pattern-reconfigurable patch antenna with CSRR on the ground," *IEEE Antennas Wireless Propag. Lett.*, vol. 16, pp. 416–419, 2017.

[13] X. Ding, Z. Zhao, Y. Yang, Z. Nie, and Q. H. Liu, "A low-profile and stacked patch antenna for pattern-reconfigurable applications," *IEEE Trans. Antennas Propag.*, vol. 67, no. 7, pp. 4830–4835, Jul. 2019.

[14] G. Jin, M. Li, D. Liu, and G. Zeng, "A simple four-beam reconfigurable antenna based on monopole," *IEEE Access*, vol. 6, pp. 30309–30316, 2018.

[15] M. S. Alam and A. M. Abbosh, "Wideband pattern-reconfigurable antenna using pair of radial radiators on truncated ground with switchable director and reflector," *IEEE Antennas Wireless Propag. Lett.*, vol. 16, pp. 24–28, 2017.

[16] M. C. Jose, R. C. Devi, B. Sreeja, S. Meraline, and S. Radha, "A novel wideband pattern reconfigurable antenna using switchable parasitic stubs," *Microw. Opt. Technol. Lett.*, vol. 61, no. 4, pp. 1090–1096, 2019.

[17] A. Ghaffar *et al.*, "A flexible and pattern reconfigurable antenna with small dimensions and simple layout for wireless communication systems operating over 1.65-2.51 GHz," *Electronics*, vol. 10, no. 5, p. 601, Mar. 2021.

[18] Y. P. Selvam *et al.*, "A low-profile frequency-and pattern-reconfigurable antenna," *IEEE Antennas Wireless Propag. Lett.*, vol. 16, pp. 3047–3050, 2017.

[19] S. A. Haydhah, F. Ferrero, L. Lizzi, M. S. Sharawi, and A. Zerguine, "A multifunctional compact pattern reconfigurable antenna with four radiation patterns for sub-GHz IoT applications," *IEEE Open J. Antennas Propag.*, vol. 2, pp. 613–622, 2021.

[20] H. Tian, K. Dhwaj, L. J. Jiang, and T. Itoh, "Beam scanning realized by coupled modes in a single-patch antenna," *IEEE Antennas Wireless Propag. Lett.*, vol. 17, no. 6, pp. 1077–1080, Jun. 2018.

[21] B. Ashvanth, B. Partibane, M. G. N. Alsath, and R. Kalidoss, "Gain enhanced multipattern reconfigurable antenna for vehicular communications," *Int. J. RF Micro. Comput.-Aided Eng.*, vol. 30, no. 6, Mar. 2020, Art. no. e22192.

[22] Y.-H. Ke, L.-L. Yang, and J.-X. Chen, "Design of switchable dual-balun feeding structure for pattern-reconfigurable endfire antenna," *IEEE Antennas Wireless Propag. Lett.*, vol. 20, no. 8, pp. 1463–1467, Aug. 2021.

[23] H.-Y. Cheng and J.-S. Row, "A design for pattern reconfigurable antenna systems," *Microw. Opt. Technol. Lett.*, vol. 63, no. 6, pp. 1760–1766, Feb. 2021.

[24] R. Garg, P. Bhartia, I. J. Bahl, and A. Ittipiboon, *Microstrip Antenna Design Handbook*. Boston, MA, USA: Artech House, 2001.

[25] J. J. Adams and J. T. Bernhard, "Broadband equivalent circuit models for antenna impedances and fields using characteristic modes," *IEEE Trans. Antennas Propag.*, vol. 61, no. 8, pp. 3985–3994, Aug. 2013.

[26] K. Michalski and L. Pearson, "Equivalent circuit synthesis for a loop antenna based on the singularity expansion method," *IEEE Trans. Antennas Propag.*, vol. 32, no. 5, pp. 433–441, May 1984.

[27] A. B. Abdel-Rahman, A. K. Verma, A. Boutejdar, and A. S. Omar, "Control of bandstop response of Hi-Lo microstrip low-pass filter using slot in ground plane," *IEEE Trans. Microw. Theory Techn.*, vol. 52, no. 3, pp. 1008–1013, Mar. 2004.

[28] W. A. Awan *et al.*, "Design and realization of afrequency reconfigurable antenna with wide, dual, and single-band operations for compact sized wireless applications," *Electronics*, vol. 10, no. 11, p. 1321, May 2021.

YU LIU was born in Guizhou, China, in 1999. She received the bachelor's degree in electronic information science and technology from the Changsha University of Science and Technology, Changsha, China, in 2020, where she is currently pursuing the master's degree in electronic information. Her research interests include reconfigurable antenna, electromagnetic metamaterials, and miniaturized microstrip antenna.

LI-AN BIAN was born in Tianjin, China, in 1985. He received the B.Sc. degree in electronic science and technology from Tianjin Polytechnic University in 2010, the M.Sc. degree in electromagnetic field and microwave technology from Tianjin University, Tianjin, China, in 2013, and the Ph.D. degree in electronic science and technology from the National University of Defense Technology, Changsha, China, in 2018.

He is currently with the Changsha University of Science and Technology. His research interests include antenna design and electromagnetic protection.

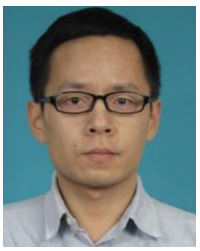

KAI-DA XU (Senior Member, IEEE) received the B.E. and Ph.D. degrees in electromagnetic field and microwave technology from the University of Electronic Science and Technology of China (UESTC), Chengdu, China, in 2009 and 2015, respectively.

From 2012 to 2014, he was a Visiting Researcher with the Department of Electrical and Computer Engineering, Duke University, Durham, NC, USA, under the financial support from the China Scholarship Council. In 2015, he joined the Department of Electronic Science, Xiamen University, Xiamen, China, as an Assistant Professor. From 2016 to 2017, he was a Postdoctoral Fellow with the State Key Laboratory of Millimeter Waves, City University of Hong Kong, Hong Kong. From 2018 to 2019, he was an Honorary Fellow with the Department of Electrical and Computer Engineering, University of Wisconsin–Madison, Madison, WI, USA. He was successfully selected into the "Youth Talent Support Program" of Xi'an Jiaotong University (XJTU) in May 2019, and joined the School of Information and Communications Engineering, XJTU in January 2020. Also, he was awarded a fellowship from the Japan Society for the Promotion of Science (JSPS) and was the JSPS Fellow with the Department of Communications Engineering, Graduate School of Engineering, Tohoku University from November 2019 to May 2021. He has authored and coauthored over 130 papers in peer-reviewed journals and over 50 papers in conference proceedings. His current research interests include RF/microwave, mm-wave/THz devices, and antenna arrays.

Dr. Xu received the UESTC Outstanding Graduate Awards in 2009 and 2015, respectively. He was a recipient of the National Graduate Student Scholarship in 2012–2014 from the Ministry of Education, China. Since 2017, he has been serving as an Associate Editor for the IEEE ACCESS and *Electronics Letters*. He has also served as an Editorial Board Member for the *AEÜ-International Journal of Electronics and Communications* and *MDPI Electronics*.

KAICHENG HUANG was born in Hunan, China, in 1997. He received the bachelor's degree in communication engineering. He is currently pursuing the master's degree in electronic science and technology with the Changsha University of Science and Technology, Changsha, China. His research interests include reconfigurable antenna, electromagnetic metamaterials, and metamaterial antennas.

YAOKUN WANG received the bachelor's degree in electronic information science and technology from the Chongqing University of Technology, Chongqing, China, in 2018. He is currently pursuing the master's degree in electronic information with the Changsha University of Science and Technology, Changsha, China. His research interests include coding metamaterials and antenna arrays.

YANXIU LI received the bachelor's degree in electronic information science and technology from the Changsha University of Science and Technology, Changsha, China, in 2021, where she is currently pursuing the master's degree in electronic science and technology. Her research interests include microstrip antenna and MIMO antenna.

SHU XIE was born in Hunan, China, in 1999. She received the bachelor's degree in electronic information science and technology from the Changsha University of Science and Technology, Changsha, China, in 2022. Her current research interests include artificial electromagnetic surface, electromagnetic protection, and antenna design.